Environmental Science
Water Research & Technology

Organic structure and solid characteristics determine reactivity of phenolic compounds with synthetic and reclaimed manganese oxides

Journal:	*Environmental Science: Water Research & Technology*
Manuscript ID	EW-ART-09-2019-000859.R1
Article Type:	Paper

Manganese oxides may enhance phenolic contaminant removal in passive *in situ* treatment systems. This study investigates the interactions between organic structure and solid characteristics, comparing synthetic δ-MnO_2 with two reclaimed oxides found to degrade a suite of phenols. Organic structure controls the relative rates and mechanisms of oxidation while reactant complexity decreases the utility of QSARs in this system.

Organic structure and solid characteristics determine reactivity of phenolic compounds with synthetic and reclaimed manganese oxides

*Emma Leverich Trainer,[1] Matthew Ginder-Vogel,[1,2]† and Christina K. Remucal[1,2]**

[1]Environmental Chemistry and Technology

University of Wisconsin - Madison

Madison, Wisconsin 53706

[2]Civil and Environmental Engineering

University of Wisconsin - Madison

Madison, Wisconsin 53706

† Corresponding author address: 660 N. Park St., Madison, WI 53706; e-mail: mgindervogel@wisc.edu; telephone: (608) 262-0768; fax: (608) 262-0454; Twitter: @profmattgv.

* Corresponding author address: 660 N. Park St., Madison, WI 53706; e-mail: remucal@wisc.edu; telephone: (608) 262-1820; fax: (608) 262-0454; Twitter: @remucal

Abstract

Manganese (Mn) oxides have been proposed for *in situ* treatment of organic (e.g., phenolic) contaminants, although little is known about the reactivity of reclaimed solids that might be used as alternatives to synthetic oxides. In this study, we investigate the impacts of phenol substituents and manganese oxide properties (e.g., surface area, iron substitution) on the kinetics and mechanism of this reaction. Reclaimed solids from acid mine drainage and drinking water treatment systems contain Mn(IV) and are capable of oxidizing phenolic contaminants, although their reactivity is 1 – 3 orders of magnitude slower than synthetic δ-MnO_2. Both electron transfer-limited and sorption-limited mechanisms occur in 29 phenols reacted with the three manganese oxide materials. This finding contrasts the common assumption that the first one-electron transfer from the phenol to the manganese oxide is rate-limiting. The occurrence of both mechanisms has implications for the rates and products of phenol oxidation. Interestingly, the mechanism for a given phenol changes between solids. We attribute this observed mechanism shift primarily to phenolic substituent effects, with influences from the pH_{pzc}, surface area, and iron substitution of the manganese oxide materials. In addition, we investigate the predictive utility of quantitative structure-activity relationships, as these models have not been tested using complex reactants and non-synthetic manganese oxides. In-depth analysis and external validation measures indicate these common QSAR models are ineffective at predicting the behavior of complex contaminants or reactions with non-synthetic manganese oxides, and therefore have limited application for predicting contaminant oxidation by manganese oxides in environmental and engineered systems.

Introduction

Manganese (Mn) oxides (e.g., MnO_2) are ubiquitous, strong oxidants that control the fate of redox active inorganic (e.g., arsenic) and organic (e.g., anilines, phenols) contaminants[1-11] in surface waters[1, 3] and soils.[1, 2, 9, 12-15] Mn oxides form naturally and are also generated as byproducts in water treatment systems that use pyrolusite filters to remove dissolved Mn and iron (Fe), as well as in acid mine drainage remediation systems that precipitate Mn on passive limestone or coir fiber beds.[16-18] Mn oxides may coprecipitate with Fe and other non-Mn species (e.g., Zn, Al, silica) or comprise a fraction of a heterogenous mixture, as in the case of natural soils. As a result, Mn oxides exhibit a wide range of characteristics (e.g., surface area, Mn oxidation state) that alter their reactivity compared to synthetic materials.[2, 4, 7, 19-21] Contaminants that react with Mn oxides are present in many anthropogenic systems that discharge to natural environments, where they are typically recalcitrant and often threaten ecosystem and human health.[1, 22-26] Therefore, Mn oxides have been proposed for passive, *in situ* treatment of contaminated waters. Such applications are particularly attractive for reclaimed solids as inexpensive alternatives for the treatment of phenolic contaminants in wastewater effluents, landfill leachates, or stormwater basins. However, there is a lack of research bridging well-controlled, microscopic studies with *in situ* macroscopic investigations.

Phenols react with Mn oxides through a series of one-electron transfers, first forming a phenoxy radical which can either desorb from the manganese surface reaction site and couple to form a polymeric product or undergo a second one-electron transfer to form benzoquinone-like products.[1, 6] The phenol oxidation reaction is more nuanced than this generalized pathway details, as hydrogen abstraction, coupled proton-electron transfer, and desorption processes may obscure the rates of sorption and electron transfer.[29-31] However, there is no clear experimental evidence

that these processes control oxidation rates in this system. Thus, this work follows the simplified theory that either the first one-electron transfer or sorption of the phenolate ion limits the overall oxidation rate, resulting in one or two electron transfers, respectively.[1, 6, 27, 28] The overall reaction mechanism, identified by the rate-limiting step, dictates both the rate of reaction and final oxidation products (i.e., benzoquinone or polymeric products).[1, 32-34] The influence of reclaimed Mn oxide characteristics (e.g., surface area, Fe content) on the rates and mechanism of phenol oxidation are unknown.

The oxidation of organic compounds by Mn oxides is frequently investigated with a limited set of simple phenols and well-characterized synthetic manganese oxides (e.g., δ-MnO_2).[6, 11, 27, 34-44] These highly controlled studies then use quantitative structure-activity relationships (QSARs) to describe trends in the reactivity of Mn(III/IV) oxides with anilines[1, 38, 39, 41] and phenols.[1, 6, 29] QSARs are simple models relating descriptive molecular parameters and structural properties to reactivity to predict reaction rate constants of related compounds, determine differences in reaction mechanisms between groups of compounds (e.g., phenols versus phenolates) or oxidants, or provide other insights into the reaction system.[29, 30, 45-48] However, previous studies applying these models to predict organic oxidation rates by manganese oxides do not test the applicability in complex environmental systems. Notably, the acceptance of QSAR models is not grounded in external validation techniques, but rather on basic linear regression statistics. Importantly, there is a lack of data for isomeric sets of phenols (i.e., *ortho-, meta-,* and *para-*), complex phenols (e.g., triclosan, 17β-estradiol), and non-synthetic manganese oxides.

In this study, phenols ranging in complexity from simple model compounds to complex contaminants and metabolites are reacted with synthetic δ-MnO_2 and two reclaimed sources of Mn oxides to investigate how organic structural properties and solid phase characteristics

mechanistically alter reactivity. In addition, we assess whether QSARs can overcome the complexities expected in environmental systems to which such QSAR models may be applied. To do this, we first compare the oxidation rates and rate-limiting steps of 29 phenols reacted with δ-MnO_2 and verify the results with kinetic models. Second, we react selected phenols with two reclaimed Mn oxides to determine the impact of Mn structural changes on reactivity and oxidative mechanism. Finally, we construct QSARs using general and specific structural descriptors to assess their utility as a predictive tool for complex contaminants using external validation measures. This work combines complementary aqueous and solid-phase analyses to demonstrate how both complex contaminants and non-synthetic solids mechanistically alter phenol degradation by Mn oxides, with implications for oxidation rates and products. In addition, we show that previous literature QSARs built for this system have little predictive utility outside of simple, well-controlled laboratory studies.

Experimental

Materials. Commercial chemicals were used as received (Electronic Supplementary Information **Section S1**). Phenol stock solutions were prepared in methanol and stored at 4 ^{o}C. Ultrapure water was supplied by a Milli-Q water purification system maintained at 18.2 MΩ·cm.

δ-MnO_2 was synthesized by a modified Murray method (**Section S1**).[49] Drinking water treatment (DWT) solids were collected from a Mn removal system at Well 29 in Madison, WI, operated by Madison Water Utility. Acid mine drainage (AMD) remediation solids were collected by Hedin Environmental from a passive limestone Mn removal bed in western Pennsylvania.[16] Both reclaimed solids were pre-equilibrated in pH 5.5 10 mM sodium acetate buffer over four days at 4 ^{o}C to remove carbonate phases and stabilize the solution pH prior to reaction with phenols.

Solid Characterization. δ-MnO_2, DWT, and AMD starting materials were characterized to determine average manganese oxidation number (AMON) by X-ray absorption near edge spectroscopy (Mn K edge; 6532 eV).[50] Specific surface area was determined by Brunauer–Emmett–Teller measurements (Quantachrome Autosorb-1, nitrogen adsorbate; 30 ^{o}C). The solids were also characterized by X-ray diffraction (Rigaku Rapid II, Mo Kα source; λ = 0.7093 Å) and scanning electron microscopy (LEO 1530, Schottky-type field-emission electron source). Sodium (δ-MnO_2) or trace metal (DWT and AMD solids) content was quantified by dissolution in HCl followed by inductively coupled plasma-optical emission spectrometry (ICP-OES; Perkin Elmer 4300). The pH of zero charge values (pH_{pzc}) were determined by rapid potentiometric titration.[51, 52] Details are provided in **Section S2**.

Kinetic Reactions. Triplicate batch reactions of each target phenol (10 μM; <0.1% methanol) and Mn oxides (15 mg-Mn/L) were conducted in pH 5.5 10 mM sodium acetate buffer. Experiments with 4-*n*-nonylphenol used a concentration of 1 μM with 1.5 mg-Mn/L due to its lower solubility.[53] All experiments were conducted in the dark. This pH and buffer were selected for several reasons. Although pH 5.5 is low for most natural waters, it is relevant for AMD systems. More importantly, this pH is below the phenolic acid dissociation constant (pK_a) of all 29 phenols (**Table S8**). 2-Nitrophenol has the lowest phenolic pK_a at 6.43 (10.5% deprotonated at pH 5.5), followed by 3-trifluoromethyl-4-nitrophenol (pK_a = 6.7, 5.9% deprotonated). All other phenolic pK_a values are above 7 (<3% deprotonated), so speciation is not a driving factor of relative observed rate constants and reactivity trends described here. Furthermore, this lower pH value is also correlated with faster oxidation kinetics by Mn oxides, enabling rate determination of less reactive solids.[1, 6, 11, 35] Finally, unlike Good's buffers and phosphate,[1, 33, 35, 38, 54, 55] sodium acetate does not reduce or complex δ-MnO_2 (**Section S3**).

132 The reactors were continuously stirred for up to ten days. Two aliquots were collected at
133 each timepoint to quantify the parent phenol concentration of filtered (0.2 μM PTFE) and quenched
134 (5:1 ascorbic acid:Mn molar ratio) samples. Filtering removes all solids from the filtered aliquots,
135 including any sorbed parent phenol. In contrast, the Mn oxide and all sorbed species are dissolved
136 into solution in the acid quenched aliquots. Organic compound concentrations were quantified by
137 high performance liquid chromatography (HPLC) and used to calculate initial pseudo-first-order
138 rate constants (**Section S4**). The sorbed fraction of the parent compounds was calculated at each
139 timepoint as the difference between the total dissolved (i.e., quenched) and aqueous (i.e., filtered)
140 concentrations. Compounds with observed maximum sorption <10% or with error greater than the
141 average measured sorption were operationally defined as having reaction rates that were sorption-
142 limited, as discussed in **Section S5**. The phenols with a maximum observed percent sorption >10%
143 were classified as undergoing electron transfer-limited reactions assuming no atom transfer occurs.
144 Fifteen phenols with oxidation rates limited by either electron transfer or sorption and that
145 represent a range of structural complexity were selected for experiments with DWT and AMD
146 solids. Solids were added at a Mn normalized concentration of 15 mg-Mn L^{-1}. Quenched aliquots
147 were subsequently filtered through 0.2 μm PTFE filters to remove residual solids prior to analysis.
148 **Kinetic Modeling.** Calculated rate constants for the electron transfer-limited and sorption-
149 limited reaction pathways (*k'* and *k''*, respectively) were fit to quenched experimental data, as
150 described previously.[28] The calculated pseudo-first-order rate constant (*k'* or *k''* multiplied by the
151 initial phenol concentration) that gave a higher R^2 fit to the experimental loss curve was selected
152 for each compound and compared to observed pseudo-first-order rate constants for phenolic
153 oxidation by δ-MnO_2. Details are provided in **Section S6**.

154 **Quantitative Structure-Activity Relationship Descriptors.** Hammett constants (σ) were
155 summed from tabulated substituent group values.[56-59] These constants were only available for
156 sixteen phenols to avoid the assumption that *ortho*-substitutions are adequately described by *para*-
157 substituted values.[60] Acid dissociation constants were calculated using ChemAxxon software;[61]
158 the lowest predicted phenolic pK_a values were used.

159 Theoretical molecular calculations were computed with NWChem EMSL Arrows online
160 API service[62] using density functional theory, 6-311++G(2d,2p) basis, M06-2x cross correlation,
161 and COSMO-SMD solvation theory.[29, 41] Energy of the highest occupied molecular orbital
162 (E_{HOMO}) values were calculated for each phenol species at pH 5.5. Oxidation energy of the first
163 electron transfer (E_{ox}) was determined for the loss of the first electron from the parent phenol and
164 corrected ($E_{ox,corr.}$) to values reported by Pavitt et al.[29] (**Section S7**; **Fig. S4**).[48] All pseudo-first-
165 order rate constants were normalized to 4-chlorophenol to enable cross-study comparison.
166 Previous studies using relative rate constants further describe the convention of normalizing
167 observed rate constants to 4-chloro congeners.[41] Normalized literature pseudo-first-order rate
168 constants were adjusted to k_{obs} values where necessary and QSAR descriptors were calculated as
169 described above to ensure consistency across datasets (**Table S12**).[41]

170

171 **Results and Discussion**

172 **Kinetics and Mechanisms of Oxidation by δ-MnO_2.** We investigate the influence of
173 increasingly complex organic structure on reaction rates and oxidation mechanism by reacting 29
174 phenols with δ-MnO_2. These phenols include a range of functional group placements (i.e., *ortho*-,
175 *meta*-, or *para*-substitutions, including three isomeric sets), electron-withdrawing versus electron-
176 donating substituents, and structural complexity (**Table S2**). Initial pseudo-first-order rate

constants are fit to both total and dissolved kinetic data (i.e., quenched and filtered samples; **Table S6**). Percent sorption is calculated to experimentally determine the observed rate-limiting step (**Section S5**).

Sixteen compounds (e.g., triclosan; **Fig. 1a**) rapidly sorb to δ-MnO_2 over the initial reaction period and have a maximum observed percent sorption >13%. The degradation rates of these compounds, determined from quenched reactions, are on average 5 times slower than their removal rate from solution, indicating that sorption of these phenolic compounds to the mineral surface is more rapid than the first one-electron transfer.[1, 6, 27, 28] These compounds are rapidly removed from solution by sorption to the treatment media (δ-MnO_2), while overall degradation of the parent compound is limited by the rate of electron transfer with the Mn oxide. In contrast, degradation of the remaining thirteen phenols is sorption-limited since they show no evidence of accumulation on the manganese surface (**Table S6**).[1, 6, 27, 28] For these compounds (e.g., 4,4'-dihydroxybiphenyl, **Fig. 1b**), the measured sorbed concentration is <8% and the average ratio of filtered to quenched rate constants is 1, indicating that the total removal rate equals the rate of oxidation. Thus, these thirteen species are degraded at the same rate as they partition to the manganese surface, so the observed removal from solution is attributable to oxidation.

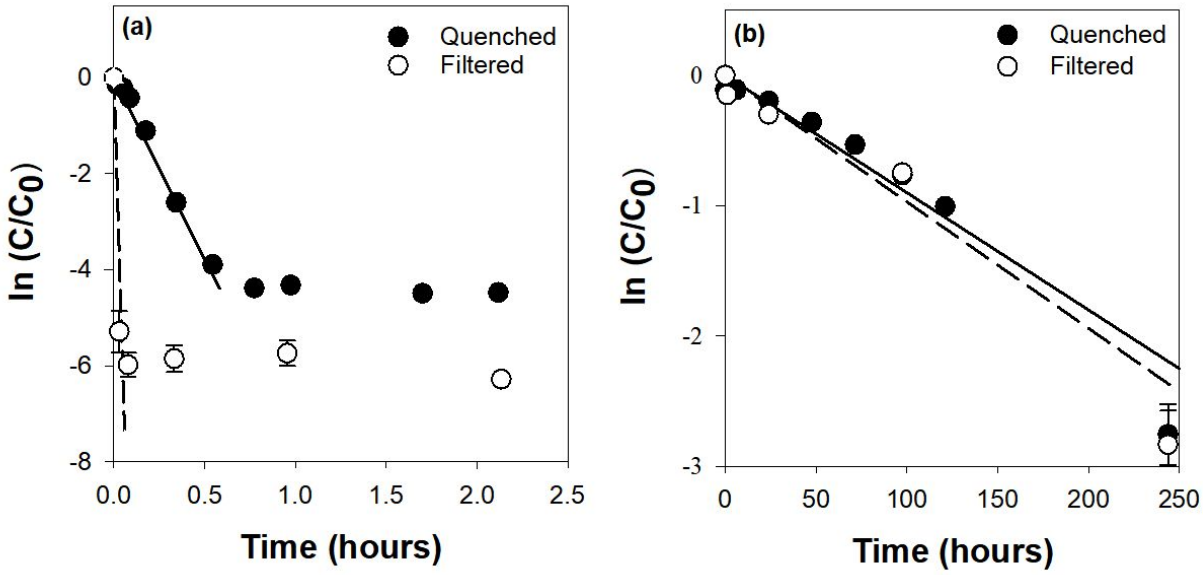

Figure 1. Kinetic data and pseudo-first-order rate fittings for (a) triclosan and (b) 4,4'-dihydroxybiphenyl based on quenched and filtered samples.

The rate-limiting step is also investigated by fitting the data with a previously developed kinetic model from Zhang et al.[28] This model separates the electron transfer- and sorption-limited reactions into two distinct equations which are both fit to the experimental kinetic data to determine the mechanism-dependent modeled pseudo-first-order rate constants, as described in **Section S6**. Modeled rate-limiting steps agree with the observed rate-limiting step for 24 of the 29 phenols. 4-Cresol, 2-chlorophenol, and 4-*n*-nonylphenol are experimentally determined to be electron transfer-limited but are better fit by the modeled sorption-limited $k''*C_0$. The opposite trend is observed for 2-nitrophenol and 4,4'-dihydroxybiphenyl. In the cases where the model and experimental rates disagree, minimal differences between the R^2 fit of modeled electron transfer-limited (i.e., k') and sorption-limited (i.e., $k''*C_0$) rate constants are observed (i.e., difference in R^2 ranging between 8.7×10^{-6} and 4.7×10^{-2}; **Table S7**). This model supports the 10% sorption cutoff used in this study and the occurrence of both operationally defined rate-limiting steps within the suite of 29 phenols reacted with δ-MnO_2 (**Section S5**).

210 Compounds with larger observed rate constants (i.e., faster oxidation kinetics) are overall
211 fit better by *k'* and are electron transfer-limited, while phenols with smaller observed rate constants
212 are better fit by *k''*$*C_0$ and are sorption-limited (**Table S7**). Interestingly, isomeric differences in
213 the rate-limiting step occur for chlorophenols, but not for nitrophenols or hydroxybenzoic acids.
214 For example, 3-chlorophenol is sorption-limited, while 2- and 4-chlorophenol are electron transfer-
215 limited. While each of these isomeric substitutions (i.e., COOH, NO_2, Cl) are electron
216 withdrawing, halogens have unique interactions (e.g., orbital overlap) with the aromatic pi-bond
217 system which may explain why chlorophenols exhibit isomeric effects not demonstrated by the
218 nitro- or carboxylate-substituted phenol isomers. Previous studies also report isomeric effects for
219 chlorophenols (i.e., primarily that *meta*-chlorophenols react slower than *ortho*- or *para*-
220 chlorophenols) and that reaction rates for all studied chlorophenols increased with increased
221 sorption to MnO_2 surfaces,[11, 63] which we attribute here to the differences in the reaction
222 mechanism between these isomers. However, there are no clear trends in substituent group effects
223 on oxidation mechanism within the overall dataset. Similarly, there are no trends with the analyzed
224 partitioning and structural properties of each compound, including the distribution ratio between
225 octanol and water (log D_{ow}), solubility, organic carbon partitioning coefficient (log K_{oc}), or van
226 der Waals' volume (**Table S8**).

227 The occurrence of both electron transfer- and sorption-limited mechanisms within the 29
228 phenols reacted with δ-MnO_2 illustrates that contaminant structure controls both the mechanism
229 and degradation kinetics when reacted with a given oxidant. This observation disagrees with the
230 commonly accepted mechanism in which the rate of phenolic compound oxidation by manganese
231 oxides is electron transfer-limited.[1, 6, 27, 28] Although evaluation of the oxidation products of the
232 large number of phenols is beyond the scope of this study, the divergence in rate-limiting steps

suggests that the relative importance of benzoquinone and polymeric degradation products will also vary across the studied phenols.

Phenol Degradation by Reclaimed Manganese Oxides. Manganese oxides that form naturally (e.g., Mn rich soils or biogenic solids) or in engineered systems are potential alternatives to synthetic minerals for passive *in situ* contaminant treatment systems. Natural and reclaimed solids are often impure, heterogenous phases containing manganese, iron, and/or other trace metals. They differ from δ-MnO_2 in crystallinity, bulk surface area and charge, and heteroatom interactions.[1, 2, 5-9, 13, 21] Therefore, these oxides likely interact with organic contaminants differently than commonly studied synthetic materials. However, it is not clear which solid-phase characteristics have the greatest impact on contaminant degradation or how the phenol oxidation mechanisms change across Mn oxide materials as the only studies comparing these factors across Mn oxides use synthetic materials.[27, 37]

To determine whether organic structure or solid characteristics control reactivity, we compare the degradation rates and mechanisms of fifteen selected phenols reacted with δ-MnO_2 and reclaimed manganese oxides from drinking water treatment and acid mine drainage remediation systems, which were chosen based on their reclamation potential for passive *in situ* treatment applications. The selected phenols vary in reactivity, identified reaction mechanisms with δ-MnO_2, and substitution. Spectroscopic analyses discussed below indicate the Mn present in all three solids is primarily discrete Mn(III/IV) oxides, as opposed to coprecipitates or surface coatings. Although these reclaimed solids are impure, we refer to all three as Mn oxides for simplicity as we test the oxidation behavior of the bulk solid as a potential source of reclaimed Mn oxides. The fifteen phenols include contaminants (e.g., estrone, bisphenol A, and triclosan) and the full isomeric set of chlorophenols (**Table S14**). The three solids (i.e., δ-MnO_2, AMD, and

DWT) are normalized in reactions to 15 mg-Mn L^{-1} and represent a range of bulk composition and structural properties (**Section S2**).[1, 2, 5-9, 13, 14, 21]

δ-MnO_2 is a poorly crystalline layered mineral; it is a well-characterized, highly reactive proxy for birnessite.[1, 35, 37, 49, 64] In contrast, the AMD and DWT solids are heterogenous (**Fig. S1**) and contain 0.2 and 42.9 weight % Fe, respectively, along with other trace metal impurities (e.g., up to 7.9 wt % Al; **Table S3**). All three solids have less than 5% organic carbon (**Section S2**). The bulk composition of AMD solids also includes crystalline phases (e.g., quartz, silica; **Fig. 2**). The surfaces of these materials highlight the variation between synthetic and non-synthetic materials. δ-MnO_2 has a higher N_2-BET surface area than DWT or AMD solids (191, 22, and 6 m^2 g^{-1}, respectively). In contrast, the DWT and AMD solids have higher average pH_{pzc} values than δ-MnO_2 (9.9 and 6.2 versus 2.2, respectively) based primarily on their additional iron content, corresponding to differences in the net surface charge at the reaction pH of 5.5. All three solids in this study have AMON values around 3.8 (**Table 1**), so reactivity differences are indicative of bulk composition and surface characteristics, rather than Mn oxidation state.[1, 5-7, 37, 64]

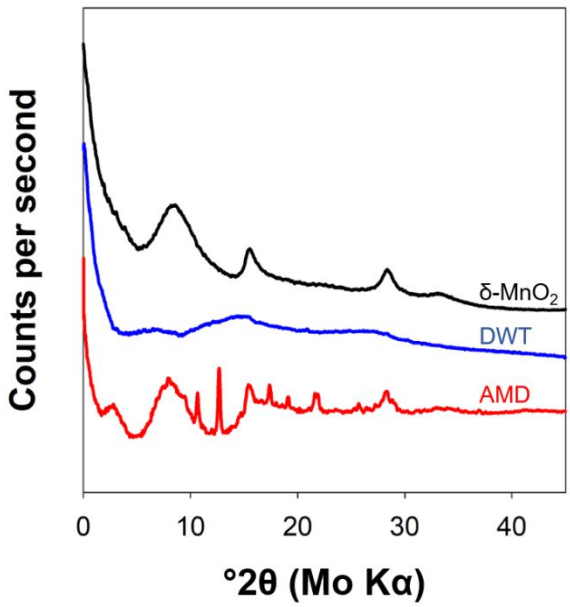

Figure 2. X-ray diffraction patterns of δ-MnO_2, drinking water treatment (DWT), and acid mine drainage (AMD) solids.

Based on the surface areas of the reclaimed oxides, these materials are expected to be less reactive than δ-MnO_2. In addition, the lower Mn content, substitution with Fe (DWT solids), or the presence of other trace metals and crystalline phases (AMD solids) points to a lower reactivity of these minerals, as Mn is a stronger oxidant than Fe or other trace metal species. Measurable oxidation did occur for each of the fifteen phenolic compounds when exposed to the reclaimed solids, demonstrating the potential for natural and reclaimed solid reuse for passive *in situ* treatment applications. Overall, DWT solids are 1 – 2 orders of magnitude less reactive and AMD solids are 1 – 3 orders of magnitude less reactive than δ-MnO_2 (**Fig. 3**; **Table S6**). For example, the quenched, pseudo-first-order oxidation rate constant for estrone is 6.0 $hour^{-1}$ with δ-MnO_2, 0.09 $hour^{-1}$ with DWT solids, and 0.01 $hour^{-1}$ with AMD solids.

Table 1. Solid phase characteristics of δ-MnO_2, DWT, and AMD solids.

	% Mn	**% Fe**	**Average Mn oxidation number**	**Surface area (m^2 g^{-1})**	**Point of zero charge**	**Surface charge at pH 5.5**
δ-MnO_2	63 ± 6	0 ± 0	3.8 ± 0.2	191	2.19 ± 0.06	Negative
DWT	8.7 ± 0.8	43 ± 2	3.82 ± 0.04	22	9.9 ± 0.2	Positive
AMD	42.8 ± 0.8	0.2 ± 0.2	3.79 ± 0.04	6	6.2 ± 0.3	Circumneutral

These observed rate constants are of similar magnitude to other studies comparing synthetic and natural soil Mn and Fe oxides. For example, one study reports 1 – 2 orders of magnitude lower percent loss for six phenolic acids reacted with Mn- and Fe-rich Palouse soil compared to MnO_2 and $Fe(OH)_3$.[65] Similarly, catechol degrades at a rate of 0.04 to 1.8 hr^{-1} with four Mn- and Fe-containing soils at pH 8 compared to about 0.1 hr^{-1} with a commercial Mn(IV) oxide.[66] These soil rates include microbial influences (e.g., re-oxidation of reduced Mn and direct microbial catechol degradation), which may explain the ten-fold faster rates of some soils

compared to commercial Mn(IV). Another study reports equal rates of diclofenac oxidation (0.2 hr^{-1}) for a biogenic manganese oxide and δ-MnO_2 at pH 4.7.[67] While these studies do not directly assess the reactivity of reclaimed materials and include a small number of target compounds, the results for biogenic and natural soil Mn oxides are similar to our finding that the reclaimed oxides degrade phenols 1 – 3 orders of magnitude slower than δ-MnO_2 without additional microbial influences.

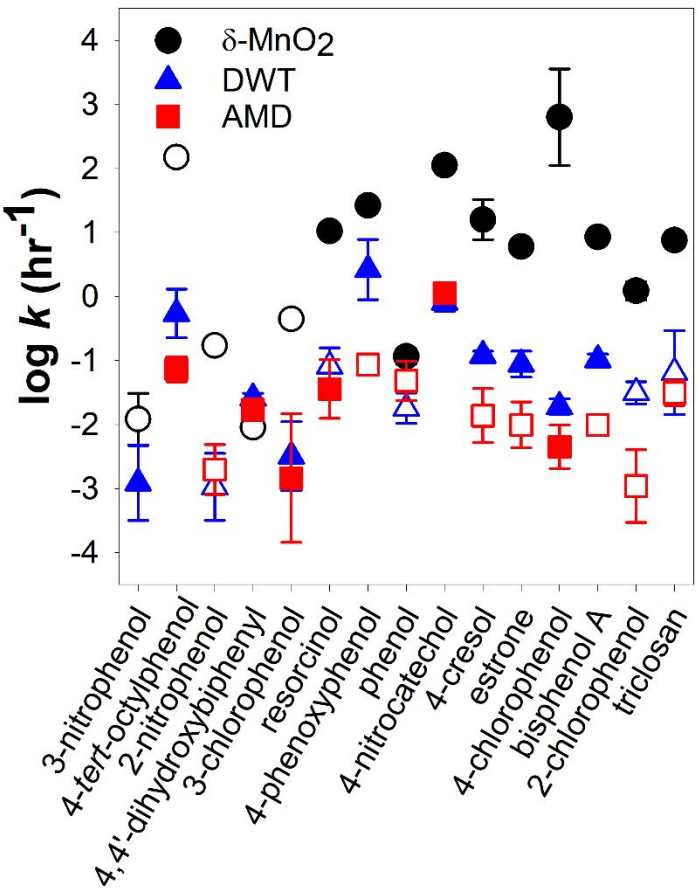

Figure 3. Initial pseudo-first-order log *k* values for reactions of 15 phenolic compounds with δ-MnO_2, drinking water treatment solids, and acid mine drainage remediation solids. Filled points are electron transfer-limited and hollow points are sorption-limited. Error bars indicate the standard deviation of triplicate data.

304 The rate-limiting step is different between the three different manganese oxides for twelve
305 of the fifteen phenols as defined by the sorption behavior of the parent phenol (**Fig. 3**; **Table S14**).
306 For example, 4,4'-dihydroxybiphenyl, 4-*tert*-octylphenol, 3-chlorophenol, and 3-nitrophenol are
307 sorption-limited with δ-MnO_2 and electron transfer-limited with both reclaimed solids. In contrast,
308 eight phenols (e.g., triclosan, phenol, 2-chlorophenol) switch from an electron transfer-limited
309 reaction with δ-MnO_2 to a sorption-limited reaction with one or both reclaimed solids. The rate-
310 limiting step does not change for the three remaining phenols; 4-nitrocatechol and 4-chlorophenol
311 remain electron transfer-limited and 2-nitrophenol remains sorption-limited across the three solids.
312 There are no clear trends in reaction mechanism with phenolic structure across the three solids.
313 The changes in reaction mechanism cannot be explained by a single parameter related to
314 either the organic compound structure (e.g., isomeric substitution, partitioning coefficients; **Table**
315 **S8**) or Mn oxide surface chemistry (e.g., surface area, pH_{pzc}; **Table 1**). Instead, the variability in
316 rate-limiting steps implies that unique interactions between each individual pair of solid and
317 organic-phase reactants influence the relative sorption and electron transfer kinetics controlling
318 the rate-limiting process. For example, although 2- and 4-chlorophenol are both electron transfer-
319 limited with δ-MnO_2, the differences in *ortho*- and *para*-substitution cause these compounds to
320 react differently with the reclaimed solids. The reaction of 2-chlorophenol is sorption-limited and
321 4-chlorophenol is electron transfer-limited with both AMD and DWT solids. While this may be
322 attributed to the unique inductive and steric hindrance effects of 2-chlorophenol, these effects do
323 not explain why triclosan, phenol, and resorcinol share the same rate limitation pattern (**Fig. 3**).
324 This is a novel result overlooked by research on a single contaminant or single solid which suggest
325 simple explanations for shifts in observed mechanisms.[27, 28, 37, 42] Past work identifies AMON,[27, 37,
326 68, 69] surface area,[37, 68, 69] or pH_{pzc}[37, 69] as the dominant reactivity-controlling characteristics of

327 synthetic manganese oxides with limited sets of organic compounds, while our study demonstrates
328 that organic structure must also be considered.

329 Since the rate-limiting step is both compound- and solid-dependent, we analyze the relative
330 number of sorption-limited and electron transfer-limited reactions with each Mn oxide (**Fig. 3**) to
331 identify which solid characteristics are most important. With δ-MnO_2, 11 of the 15 phenols are
332 electron transfer-limited, despite electrostatic repulsion of the phenolate anion (pH_{pzc} = 2.2; **Table**
333 **1**). Thus, the relatively fast sorption kinetics are likely due to the high surface area of δ-MnO_2 (191
334 m^2 g^{-1}). In contrast, only six phenols are electron transfer-limited with AMD solids even though
335 the circumneutral net surface charge (pH_{pzc} = 6.2) should be more attractive toward the phenolate
336 anion than δ-MnO_2. The reactive surface area of AMD solids (6 m^2 g^{-1}) is 30 times smaller than
337 that of δ-MnO_2, which may explain the shift towards sorption-limited kinetics despite increased
338 electrostatic attraction. AMD solids also contain incorporated crystalline phases (e.g., quartz,
339 silica; **Fig. 2**) and trace metal impurities (e.g., Zn, Ni; **Table S3**), which decrease the concentration
340 of available manganese surface sites and further slow the relative sorption rate.

341 Ten phenols are electron transfer-limited with DWT solids. Although the relatively low
342 surface area (22 m^2 g^{-1}) is similar to AMD solids, the large Fe content and resultingly high pH_{pzc}
343 (i.e., 9.9; **Table 1**) enhance sorption to the bulk surface. Fe surface sites have a higher sorption
344 potential and lower oxidation potential than Mn, so phenolic compounds may favorably sorb to
345 these Fe surface sites without undergoing oxidation by Fe.[2, 5, 10, 13, 14, 44, 70] This change in surface
346 chemistry favors sorption and shifts organic oxidation by the bulk solid towards an electron
347 transfer-limited mechanism.

348 In summary, electrostatic interactions, surface area, and the presence of impurities control
349 general reactivity and influence the rate-limiting step across the Mn oxides. Bulk characteristics

350 (e.g., elemental composition, crystallinity) appear to have a larger effect on the rate of the first
351 one-electron transfer, while the surface characteristics (e.g., surface area, pH_{pzc}) influence the rate
352 of sorption. These properties also relate to the decrease in kinetics observed between δ-MnO_2 and
353 the reclaimed solids because each of the selected 15 phenols are 1 – 3 orders of magnitude less
354 reactive with DWT and AMD solids than with δ-MnO_2. The reclaimed solids have a lower Mn
355 content, higher Fe and impurity content, smaller surface area, and larger pH_{pzc} values than δ-MnO_2.
356 Additionally, the DWT solids are generally more reactive than the AMD solids (**Fig. 3**), which
357 implies that larger surface area and/or lower crystallinity may be the primary driver of the observed
358 oxidation rate trends between the three solids. Although the role of organic compound structure
359 cannot be linked to a specific structural descriptor, it contributes to some of the variability in
360 reactivity, as discussed below.

361 **QSAR Analysis for Synthetic and Reclaimed Mn Oxides.** To assess the extent to which
362 organic structure controls reactivity across the three studied Mn oxides, we analyze differences
363 between structural groups and solid oxidants using quantitative structure activity relationships.
364 Linear QSARs relating normalized rate constants to organic structural properties are successful at
365 predicting the reactivity of *meta*- and *para*-substituted phenols and anilines with synthetic
366 manganese oxides,[1, 6, 29, 39, 41, 71] yet their utility outside of reactions between synthetic Mn oxides
367 and simply substituted model compounds is untested. We evaluate the strength of QSARs with 27
368 phenols; hydroquinone and 2,5-dihydroxybenzoate are excluded from QSAR development due to
369 indeterminable quenched rate constants (**Section S4**). The 27 phenols are separated into three
370 groups. The first group includes *meta*- and *para*-substituted phenols, which are commonly studied
371 and for which structural descriptors are readily available. The second group includes *ortho*-
372 substituted phenols, which are more difficult to accurately describe with general molecular

373 descriptors (e.g., Hammett constants) due to intramolecular interactions and steric hinderance.[6, 41, 45, 60, 71] *Ortho*-substituted compounds are less common in mechanistic studies of phenol oxidation
375 by manganese oxides and studies that include these compounds typically focus on substituted
376 chlorophenols.[6, 11, 34, 40] The final group includes complex phenols, which are also difficult to
377 predict by molecular descriptors as they contain multiple aromatic rings or large, branched
378 functional groups. These phenols are not typically included in multi-compound reactivity studies
379 but are common environmental contaminants.[1, 6, 11, 39-41]

380 General molecular descriptors used in the development of QSARs include Hammett
381 constants (σ) and pK_a values.[39, 56-59, 71] Hammett constants are available for sixteen compounds,
382 while predicted pK_a values are calculated for all 27 phenols. Electron-withdrawing substituents
383 (i.e., denoted by positive σ and correspondingly low pK_a) decrease electron density on the phenolic
384 moiety, making the phenol group less susceptible to oxidation.[39, 41, 56, 60, 71] Thus, phenolic
385 oxidation rates are expected to increase with decreasing Hammett constants and increasing pK_a.[39,
386 41, 57, 60, 71] QSARs developed with Hammett constants and pK_a values for δ-MnO_2 follow the
387 expected trends (**Figs. 4a** and **4b**), although the goodness of the fit (e.g., R^2 and p-values) of the
388 linear relationship decreases as phenol complexity increases (**Table S9**). QSARs developed with
389 Hammett constants inherently select for simple compounds due to the lack of tabulated values for
390 complex substituents,[30, 41, 47] therefore Hammett constants are not a realistic descriptor to predict
391 complex contaminant reactivity in this system, despite the strong linear regression ($p = 0.00022$
392 for *meta*- and *para*-phenols; **Fig. 4a**). The pK_a-dependent QSAR also fails to accurately account
393 for complex substituents. Although the regressions are significant at $p < 0.05$, the linear relationship
394 contains visible scatter even for *meta*- and *para*-substituted compounds (**Fig. 4b**; **Table S9**).

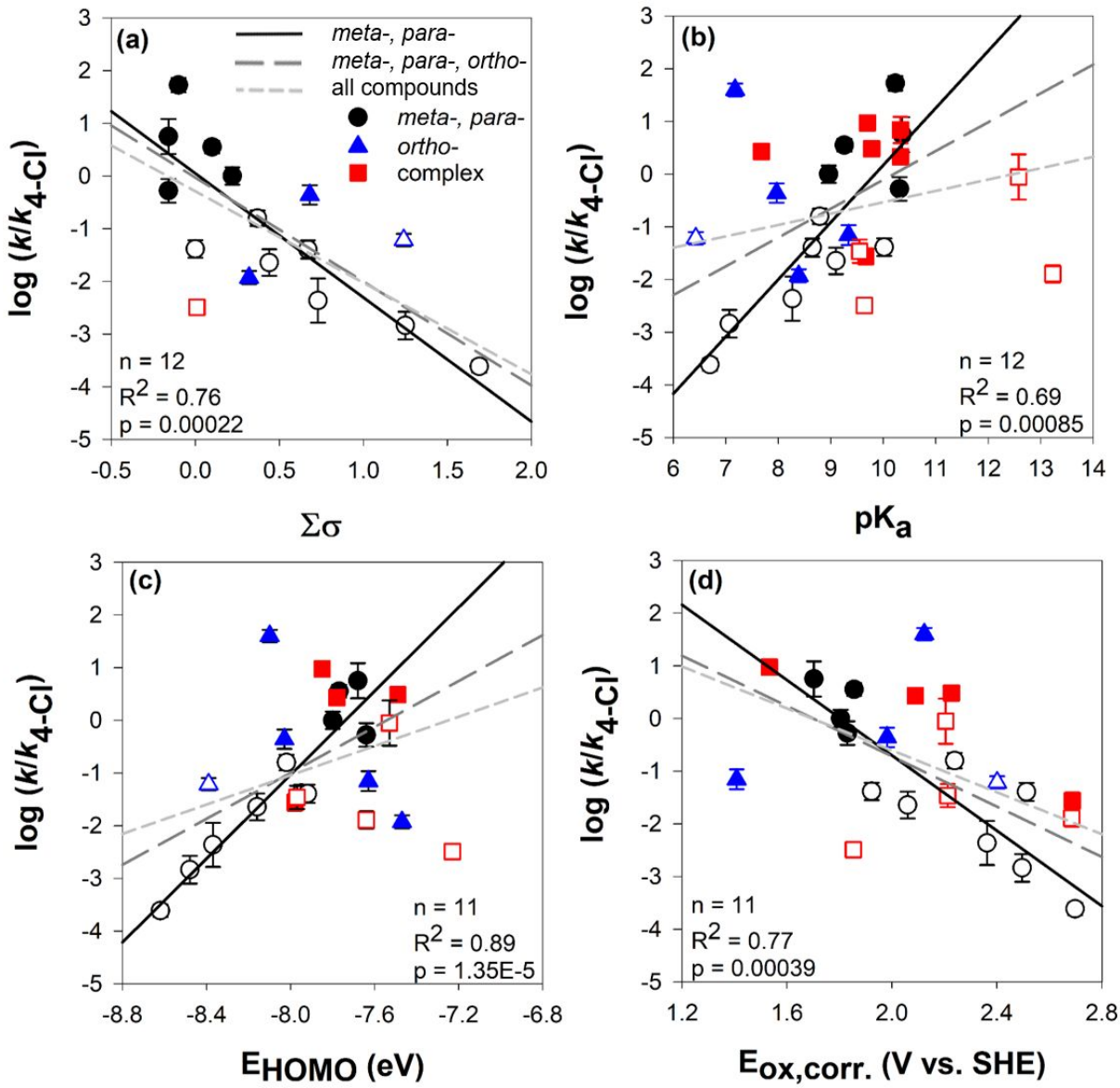

Figure 4. The log of the quenched pseudo-first-order rate constant of 29 target phenolic compounds reacted with δ-MnO_2 normalized to the rate constant of 4-chlorophenol versus (a) sum of the tabulated Hammett constants, (b) first phenolic pK_a, (c) energy of the highest occupied molecular orbital, and (d) corrected oxidation energy of the first electron transfer. Error bars indicate the standard deviation of triplicate data. Filled data points indicate electron transfer-limited mechanisms and hollow data points indicate sorption-limited reaction mechanism. Regression values are for the simple *meta*- and *para*-substituted phenols; regression values for all lines are given in **Table S9**. Experiments were conducted with 10 μM phenol and 15 mg/L δ-MnO_2 in 10 mM acetate at pH 5.5.

406 Unlike general structural properties determined from substituent groups, the energy of the
407 highest occupied molecular orbital (E_{HOMO}) and corrected one-electron oxidation potential
408 ($E_{ox,corr.}$) values are calculated for the molecule of interest and account for intramolecular
409 interactions not explained by Hammett constants and pK_a values.[30, 45, 60] This study uses
410 NWChem's open source API[62] to calculate E_{HOMO} and E_{ox} values for 24 and 23 phenols,
411 respectively. This computational database is an ideal tool for molecular contaminant fate
412 predictions than traditional software due to its increased accessibility, but it does not currently
413 contain all 27 species. E_{HOMO} is related to the inverse of ionization potential, so compounds with
414 larger values will lose an electron more easily and have faster oxidation rate constants.[30, 41, 45, 60,
415 71] The strong linear regression (**Fig. 4c**; $p = 1.3 \times 10^{-5}$ for *meta*- and *para*-substituted phenols)
416 follows the expected positive trend. In contrast, higher $E_{ox,corr.}$ is significantly correlated with lower
417 oxidation rate constants (**Fig. 4d**; **Table S9**) as the increasing energy required for oxidation of the
418 first electron slows reaction rates with Mn oxides. This correlation is not as strong as the
419 correlation of E_{HOMO} or Hammett constants for *meta*- and *para*-substituted compounds ($p =$
420 0.0004). However, $E_{ox,corr.}$ is the best descriptor for modeling complex phenols based on the
421 availability of data and low p-value ($p = 0.0082$ for all phenols; **Table S9**).

422 These linear regression results are expected based on literature model trends and first
423 principles of phenol oxidation.[11, 29, 30, 41, 45, 47, 48, 60] However, without identifying the rate-limiting
424 steps of each reaction, studies cannot delve further into the structural and mechanistic trends
425 present in these QSAR models.[30, 45, 47] Qualitatively, all four descriptors illustrate the clear
426 separation between the faster electron transfer-limited reactions and the slower sorption-limited
427 reactions with δ-MnO_2. As a result, in these well-controlled investigations of phenol oxidation by
428 synthetic δ-MnO_2, QSARs illuminate the influence of substituent effects on the rate-limiting steps

429 of reaction. Phenols that are sorption-limited with δ-MnO_2, and thus have lower observed rate
430 constants, are those with high Hammett constants, low pK_a values, low E_{HOMO} values, and high
431 $E_{ox,corr.}$ values. Thus, the sorption-limited compounds have electron-withdrawing substituents,
432 have less electron density on the phenolic group, and have greater oxidation potential energies.
433 The relationship between the rate-limiting step and the observed pseudo-first-order rate constants
434 suggests that organic structure is a major factor influencing the reaction mechanism with δ-MnO_2.

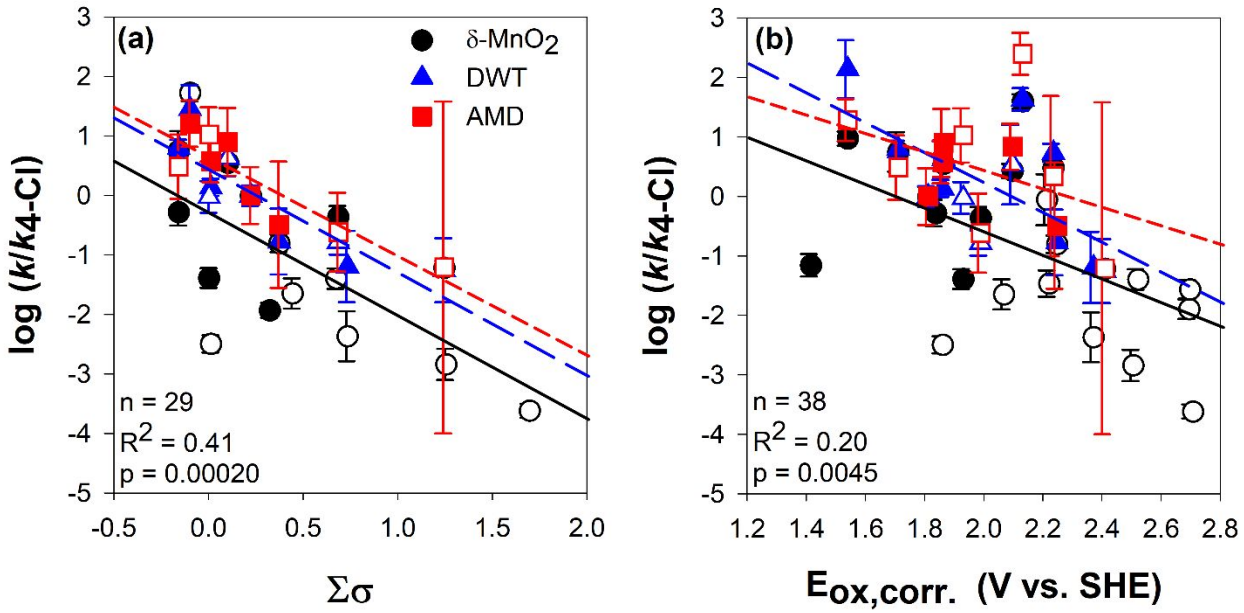

435

436 **Figure 5.** Quantitative structure-activity relationships for 15 phenols reacted with drinking water
437 treatment and acid mine drainage remediation reclaimed solids and 29 phenols reacted with δ-
438 MnO_2, all normalized to 15 mg-Mn L^{-1}. Plots show the log of the quenched rate constant
439 normalized to the rate constant of 4-chlorophenol versus (a) sum of the tabulated Hammett
440 constants and (b) corrected oxidation energy of the first electron transfer. Error bars indicate
441 standard deviation of triplicate measurements. Filled data points indicate electron transfer-limited
442 mechanisms and hollow data points indicate sorption-limited reaction mechanism. Lines indicate
443 regression fits through each solid. Regression values for all 15 phenols with each manganese oxide
444 are given in **Table S11**.

445 Furthermore, increasing compound complexity results in deviations away from the strong
446 linear relationship developed for simple *meta*- and *para*-substituted compounds (**Fig. 4**). Although
447 the QSAR correlations remain significant in all cases except for E_{HOMO}, the addition of *ortho*-

448 substituted and complex phenols lowers the R^2 39 – 85% and increases p-values by 1 – 3 orders
449 of magnitude compared to *meta*- and *para*-substituted phenols reacted with δ-MnO_2 (**Table S9**).
450 While QSARs previously developed using simple phenols or anilines reacted with δ-MnO_2 result
451 in strong correlations and support the utility of these relationships,[29, 39, 41, 71] our dataset developed
452 with structurally varied phenols shows that QSARs are ineffective for *ortho*-substituted and
453 complex phenols. While the limited utility of QSARs for complex phenols is generally assumed,
454 this assumption has not been previously tested in the Mn oxide literature.

455 QSAR plots constructed based on the kinetics of AMD and DWT solids (**Fig. 5**) show the
456 same trends as observed for δ-MnO_2. This result is unexpected given the orders of magnitude rate
457 differences and mechanism shifts between the investigated manganese oxides, as previous studies
458 demonstrate potential mechanism-dependent linear trends in QSARs developed for organic
459 contaminant oxidation by a variety of oxidants.[30, 47] The linear relationships are less significant
460 than with δ-MnO_2, with only Hammett constants ($p = 0.0002$) and $E_{ox,corr.}$ ($p = 0.0045$; **Table S11**)
461 giving significant linear correlations across all solids. Unlike the QSAR trends for the 27 phenols
462 reacted with δ-MnO_2, the separation between electron transfer-limited and sorption-limited
463 relative rate constants is not distinctive in DWT and AMD solids (**Fig. 5**). The lack of a distinct
464 separation between electron transfer- and sorption-limited rate constants highlight how the two
465 reclaimed solids behave differently than synthetic δ-MnO_2 beyond the 1 – 3 orders of magnitude
466 rate differences. This indicates that structural properties are important determinants of the reaction
467 mechanism across Mn oxides and, importantly, that synthetic oxides may not predict the reactivity
468 of reclaimed solids. However, the inconsistent shifts in the rate-limiting step between the three
469 solids for each of the 15 phenols (**Table S14**), as well as the consistent QSAR trends with structural

descriptors (**Fig. 5**), suggests that organic structure may have a greater influence on oxidation rates and overall reactivity than Mn oxide characteristics.

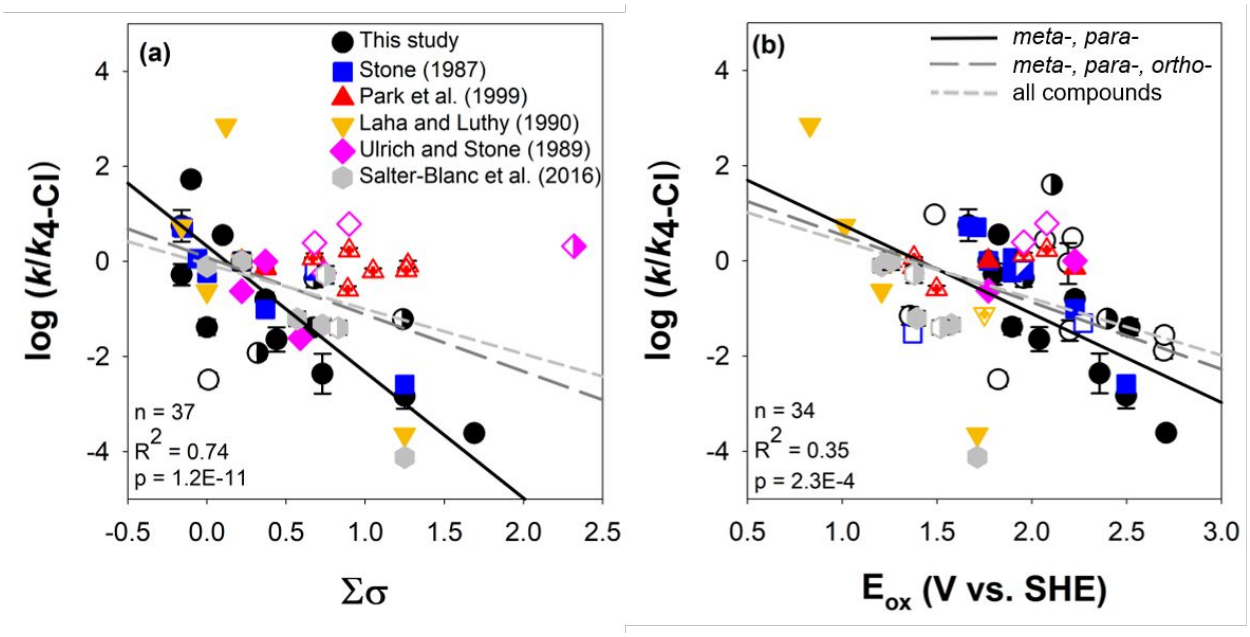

Figure 6. Quantitative structure-activity relationships for literature normalized rate constants of phenols and anilines reacted with synthetic manganese oxides[6, 11, 39-41] and reactions from this study with δ-MnO_2. The log of the average observed rate constant normalized to the rate constant of 4-chlorophenol or 4-chloroaniline is plotted against (a) sum of Hammett constants and (b) oxidation energy of the first electron transfer. Error bars indicate the standard deviation of triplicate measurements. Filled data points indicate *meta*- or *para*-substitution, partially filled points indicate *ortho*-substitution, and hollow points indicate complex compounds. Given regression values are for the simple *meta*- and *para*-substituted compounds; regression values for all lines are provided in **Table S10**.

The ability of QSARs to predict reactivity of substituted phenols and anilines with synthetic manganese oxides is further tested by constructing QSARs using literature rate constants (**Figs. 6** and **S5**).[6, 11, 39-41] Despite differences in reaction conditions (**Table S12**), log *k* values normalized to the rate constant for 4-chlorophenol enable cross-study comparison. The resulting QSARs follow the same trends as our experimental data, with stronger correlations due to the larger data set (n = 69 versus 27). For example, p-values are 2 – 40 times higher when considering QSARs developed using all compounds as compared to only *meta*- and *para*-substituted compounds for Hammett constants, E_{HOMO}, and E_{ox}. Despite this improvement, the scatter is pronounced with

490 structural complexity in QSARs constructed using literature data. The pK_a QSAR statistics do not
491 show the same trend because QSARs were developed using both aniline and phenol species (**Fig.**
492 **S5a**). Separating this relationship by anilines versus phenols results in p-values of 2.7×10^{-4} and
493 7.5×10^{-2}, respectively (**Table S10**).

494 **Assessment of Quantitative Structure Activity Relationships.** The QSAR plots (**Figs. 4**
495 **– 6**) show significant linear relationships that follow the expected trends based on first principles
496 and literature relationships.[29, 41, 48, 70, 71] In spite of significant p-values, it is apparent that the
497 QSARs are scattered with the inclusion of more complex compounds; average R^2 values decrease
498 from 0.78 for *meta*- and *para*-compounds reacted with δ-MnO_2 to 0.26 when *ortho*- and complex
499 compounds are included. These observations directly contrast the strong linear regression statistics
500 presented in the existing literature examining phenol and aniline oxidation by Mn oxides[1, 29, 39, 41,
501 48, 70, 71] and suggest that organic structure may impact the predictive utility of these models.
502 However, linear regressions are not enough to test these qualitative results as R^2 values only
503 measure how closely the data falls to the trendline and p-values test the probability that the linear
504 correlation is random. These methods, relied upon heavily in previous QSAR studies, are
505 inadequate to demonstrate model validity and are largely limited to simple comparisons.

506 Thus, we investigate the structure-dependent systematic deviations and the validity of
507 QSAR models in order to quantify the qualitative observations described above and to test whether
508 organic structural complexities directly influence the observed non-linearity of these QSARs. First,
509 to test the impact of organic structure on the observed scatter, we analyze the residuals for both
510 the simple (e.g., *meta*-, *para*-dependent or individual solid) and the all-encompassing (e.g., all
511 phenols or all solids) regression lines for QSARs constructed using the three solids and literature
512 data (**Figs. 4 – 6**; **Section S8**). Plotting the normalized log *k* residuals for each compound against

independent descriptor parameters shows that the residuals are not randomly distributed for any tested QSAR model, but instead follow clear linear or funnel-shaped trends (**Figs. S9** and **S10**). The bimodal 's' shaped distributions of the normality plots (**Figs. S11** and **S12**) further support the observed non-random residual distributions and suggest that non-linear descriptors may fit the data better,[72] although non-linear models have limited utility for this system.[45] In addition, the log *k* terms for each organic compound are consistently overpredicted (negative residuals) or underpredicted (positive residuals) by a similar magnitude, regardless of which QSAR model is used (**Figs. 7** and **S13**). This result suggests that organic structure directly influences not only reactivity, but also the utility and predictive ability of QSARs, although there is no clear trend with substitution (i.e., simple, *ortho*-, or complex) across the residual distribution (**Fig. 7**). These residual analyses showing the non-random error distribution and systematic over- and underprediction of normalized reaction rates illustrate the problematic nature of relying on QSARs for modeling contaminant reactivity.

Second, we test the validity of the structural descriptors (e.g., Hammett constants) and the cross-application of these models using external validation methods (**Section S8**). While residual analyses demonstrate the systematic error in predicting rate constants using QSARs, we use validation statistics (e.g., R^2_{pred}, r_m^2) to quantify the data variability and compare test and training data subsets to investigate if these QSARs can be applied across compound type, studies, or Mn oxides.[73-75] All combinations of test-training subsets (e.g., this study versus literature and randomized) return results outside the accepted range except for a Hammett constant descriptor case for which the relationship is inapplicable to complex contaminants lacking tabulated constants (**Table S18**). More importantly, QSARs developed using *meta*- and *para*-substituted phenols do not accurately predict the reactivity of *ortho*- and complex phenols (**Table S18**), supporting our

536 conclusion that the behavior of commonly studied simple phenols cannot be used to predict
537 oxidation rates or otherwise describe oxidation of complex contaminants by MnO_2 due to the
538 strong influence of organic structure. Similarly, the rate constants for δ-MnO_2 are not predictive
539 of the oxidation rate constants with the two reclaimed materials (**Table S19**), demonstrating that
540 commonly collected δ-MnO_2 kinetic data cannot be extended to non-synthetic materials through
541 cross correlation analyses, further supporting the conclusion that the rate-determining step of a
542 single compound with any given oxidant is not constant.[30]

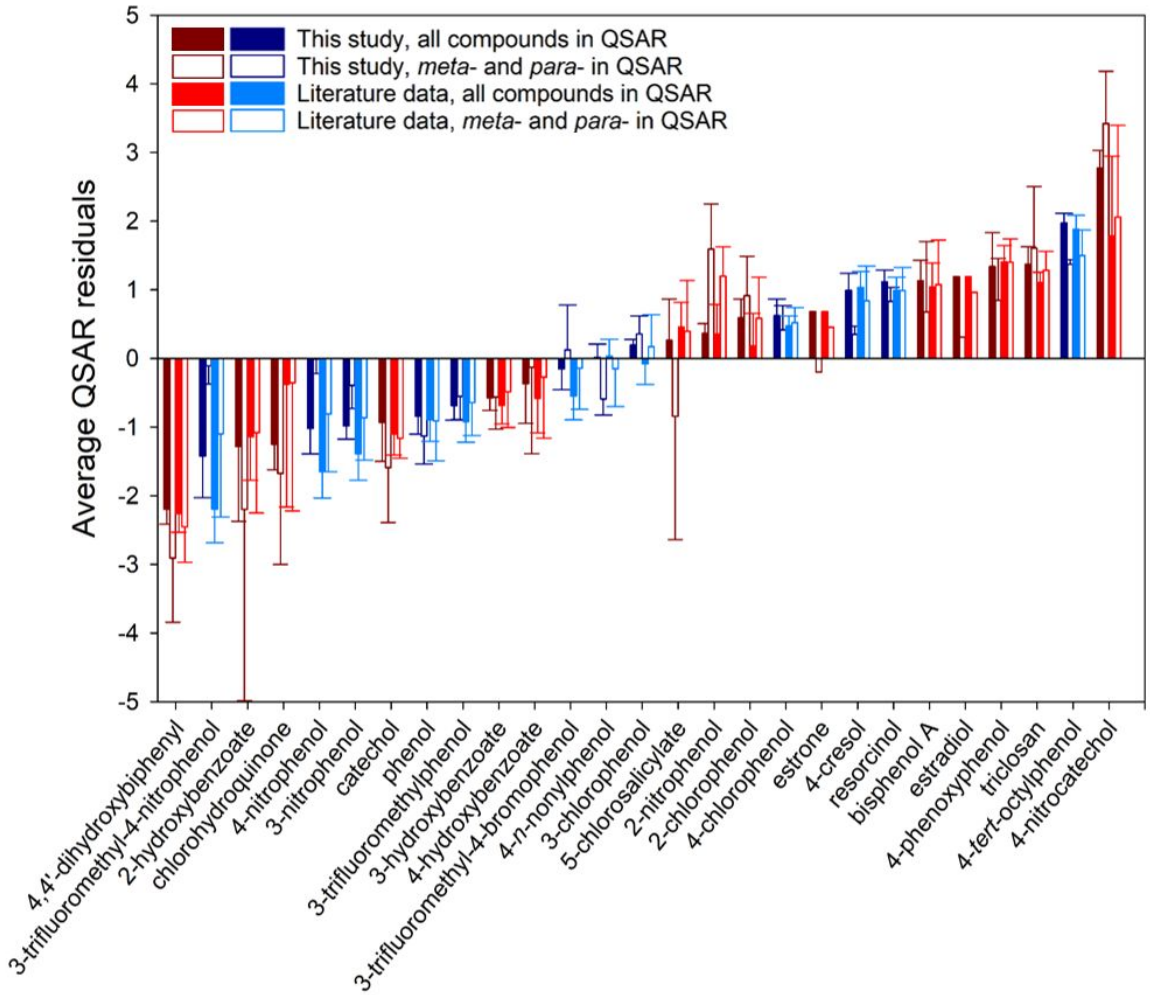

543
544 **Fig. 7.** Average residuals of Hammett constant, pK_a, E_{HOMO}, $E_{ox,corr.}$ (or E_{ox}) based QSAR models
545 developed with either all compounds or only simple *meta*- and *para*-substituted compounds, using
546 data from this study or compiled from literature. Error bars indicate one standard deviation.
547 Residual values for each QSAR model are given in **Table S15** for this study and **Table S16** for
548 literature data.

Conclusions

This study provides evidence that both sorption-limited and electron transfer-limited reaction mechanisms are observed across a wide range of phenols reacted with δ-MnO_2. The studied phenols are also oxidized by both drinking water treatment and acid mine drainage reclaimed manganese oxides, although the rate-limiting steps of reaction changes as a result of both solid-phase and organic structural characteristics. These results indicate that reclaimed Mn-containing oxide materials could potentially be applied as an alternative to synthetic materials for the *in situ* degradation of organic contaminants. By analyzing the degradation mechanism for a suite of phenols with three different solid phase oxidants, this study provides the first coupled solid and aqueous-phase insight into the complex interactions that govern both degradation rate and mechanism. We identify organic structure as the primary factor influencing the oxidation mechanism and observe that solid characteristics (e.g., iron content, surface area) also influence the relative sorption and electron transfer rates.

The mechanism by which each contaminant degrades with any given manganese oxide has implications for the *in situ* processes and rates of removal. Electron transfer-limited reactions result in relatively fast physical removal by sorption to the solid species, potentially followed by slower chemical transformation. In contrast, sorption-limited reactions are relatively slow. Since both mechanisms may occur in applied systems targeting multiple contaminants, the rates and extent of total contaminant removal from waters (e.g., by both physical sorption and chemical transformation) will differ from the rate and extent of contaminant degradation. In addition, the phenol oxidation products will differ between electron transfer-limited and sorption-limited removal pathways (i.e., polymers versus benzoquinones, respectively), which has implications for both the toxicity and environmental fate of the transformation products in treated waters.[1, 6, 27, 28]

572 Thus, both mechanisms need to be considered to accurately predict contaminant fate, removal
573 rates, and product formation in manganese oxide treatment systems.

574 Furthermore, we demonstrate that QSARs are ineffective for relating the reactivity of
575 *ortho*-substituted or complex structures (e.g., multiple aromatic rings), including contaminants of
576 environmental concern, to simple *meta*- or *para*-substituted phenols. While QSARs constructed to
577 evaluate Mn oxide reactivity are acknowledged for their predictive strength,[29, 39, 41, 71] the oxidation
578 of complex organic structures (i.e., those of key contaminants and metabolites identified in natural
579 water systems) and reclaimed solids does not follow the same linear regressions. QSAR models
580 constructed using previously identified descriptor constants (e.g., pK_a and E_{HOMO})[29, 30, 41, 45, 60] have
581 limited validity and non-random error distributions indicate these common models are not a good
582 predictor of observed rate constants for the oxidation of organic species by manganese oxides.
583 Polyparameter relationships built to incorporate multiple descriptors, data transformation, or much
584 larger datasets may improve the error distributions, validity, and fit of such QSARs.[70, 73-75]
585 However, these empirical strategies are ineffective for describing or predicting environmental
586 systems as they move away from the first principles that ground linear QSARs in well supported
587 theory and may not apply across reaction conditions.[30, 45] In addition, constructing a large enough
588 dataset that spans reaction conditions, rate-limiting processes, and oxidant characteristics to
589 potentially overcome these challenges is infeasible without dedicated data sharing platforms like
590 those available for environmental toxicology.

591 The oxidation kinetics, QSAR utility, and environmental implications (e.g., organic
592 product formation) of the system depend on the unique interactions between contaminant structure
593 and Mn oxides. Solution conditions (e.g., pH, dissolved organic matter concentration and
594 composition) are expected to further influence the kinetics of organic contaminant oxidation by

manganese oxides and warrant continued studies in increasingly complex matrices. This study highlights the necessity for studies investigating both the aqueous organic and solid phases in-depth and calls for a departure from reliance on QSARs along with the adoption of standardized model validation procedures.

Conflicts of Interest

There are no conflicts to declare.

Acknowledgements

Funding was provided by the Wisconsin Groundwater Coordinating Council and the National Science Foundation (CBET 1509879). Any opinions, findings, and conclusions or recommendations expressed in this material are those of the authors and do not necessarily reflect the views of the National Science Foundation. We acknowledge the Madison Water Utility and Robert Hedin for assistance with sample collection, Keerthana Sreenivasan for laboratory assistance, and Andrew M. Graham (Grinnell College) for helpful discussions. X-ray absorption spectroscopy was conducted at Sector 10 of the Advanced Photon Source at Argonne National Laboratory. MRCAT operations are supported by the Department of Energy and MRCAT member institutions. This research used resources of the Advanced Photon Source, a U.S. Department of Energy (DOE) Office of Science User Facility operated for the DOE Office of Science by Argonne National Laboratory under Contract No. DE-AC02-06CH11357.

Electronic Supplementary Information Available

Additional experimental details, Figures S1-S13 and Tables S1-S19 are included in the Electronic Supplementary Information.

References

1 C. K. Remucal and M. Ginder-Vogel, A critical review of the reactivity of manganese oxides with organic contaminants, *Environ. Sci. Process. Impacts*, 2014, **16**, 1247-1266.

2 O. W. Duckworth, N. A. Rivera, T. G. Gardner, M. Y. Andrews, C. M. Santelli and M. L. Polizzotto, Morphology, structure, and metal binding mechanisms of biogenic manganese oxides in a superfund site treatment system, *Environ. Sci. Process. Impacts*, 2017, **19**, 50-58.

3 J. E. Grebel, J. A. Charbonnet and D. L. Sedlak, Oxidation of organic contaminants by manganese oxide geomedia for passive urban stormwater treatment systems, *Water Res.*, 2016, **88**, 481-491.

4 J. Pena, K. D. Kwon, K. Refson, J. R. Bargar and G. Sposito, Mechanisms of nickel sorption by a bacteriogenic birnessite, *Geochim. Cosmochim. Acta*, 2010, **74**, 3076-3089.

5 J. E. Post, Manganese oxide minerals: Crystal structures and economic and environmental significance, *Proc. Natl. Acad. Sci.*, 1999, **96**, 3447-3454.

6 A. T. Stone, Reductive dissolution of manganese(III/IV) oxides by substituted phenols, *Environ. Sci. Technol.*, 1987, **21**, 979-988.

7 B. M. Tebo, J. R. Bargar, B. G. Clement, G. J. Dick, K. J. Murray, D. Parker, R. Verity and S. M. Webb, Biogenic manganese oxides: Properties and mechanisms of formation, *Annu. Rev. Earth Pl. Sci.*, 2004, **32**, 287-328.

8 M. Villalobos, B. Toner, J. Bargar and G. Sposito, Characterization of the manganese oxide produced by *Pseudomonas putida* strain MnB1, *Geochim. Cosmochim. Acta*, 2003, **67**, 2649-2662.

9 Z. Wang and D. E. Giammar, in *Advances in the environmental biogeochemistry of manganese oxides*, eds. X. Feng, W. Li, M. Zhu and D. L. Sparks, American Chemical Society, Washington, D.C., 2015, **1197**, Chapter 2, 29-50.

10 T. Borch, R. Kretzschmar, A. Kappler, P. Van Cappellen, M. Ginder-Vogel, A. Voegelin and K. Campbell, Biogeochemical redox processes and their impact on contaminant dynamics, *Environ. Sci. Technol.*, 2010, **44**, 15-23.

11 H. J. Ulrich and A. T. Stone, Oxidation of chlorophenols adsorbed to manganese oxide surfaces, *Environ. Sci. Technol.*, 1989, **23**, 421-428.

12 C. Li, B. Zhang, T. Ertunc, A. Schaeffer and R. Ji, Birnessite-induced binding of phenolic monomers to soil humic substances and nature of the bound residues, *Environ. Sci. Technol.*, 2012, **46**, 8843-8850.

13 H. Li, L. S. Lee, D. G. Schulze and C. A. Guest, Role of soil manganese in the oxidation of aromatic amines, *Environ. Sci. Technol.*, 2003, **37**, 2686-2693.

14 T. Makino, Y. Takahashi, Y. Sakurai and M. Nanzyo, Influence of soil chemical properties on adsorption and oxidation of phenolic acids in soil suspension, *Soil Sci. Plant Nutr.*, 1996, **42**, 867-879.

15 L. Schacht and M. Ginder-Vogel, Arsenite depletion by manganese oxides: A case study on the limitations of observed first order rate constants, *Soil Systems*, 2018, **2**, 39.

16 R. Hedin, T. Weaver, N. Wolfe and G. Watzlaf, presented in part at the 35th Annual National Association of Abandoned Mine Land Programs Conference, Daniels, West Virginia, 2013.

17 J. Skousen, C. E. Zipper, A. Rose, P. F. Ziemkiewicz, R. Nairn, L. M. McDonald and R. L. Kleinmann, Review of passive systems for acid mine drainage treatment, *Mine Water Environ.*, 2016, **36**, 133-153.

18 A. Reghuvaran, Biochemical aspects and formation of phenolic compounds by coir pith degraded by *Pleurotus sajor caju*, *J. Toxicol. Environ. Health Sci.*, 2012, **4**, 29-36.

19 E. R. Estes, P. F. Andeer, D. Nordlund, S. D. Wankel and C. M. Hansel, Biogenic manganese oxides as reservoirs of organic carbon and proteins in terrestrial and marine environments, *Geobiology*, 2017, **15**, 158-172.

20 I. Forrez, M. Carballa, G. Fink, A. Wick, T. Hennebel, L. Vanhaecke, T. Ternes, N. Boon and W. Verstraete, Biogenic metals for the oxidative and reductive removal of pharmaceuticals, biocides and iodinated contrast media in a polishing membrane bioreactor, *Water Res.*, 2011, **45**, 1763-1773.

21 C. M. Santelli, S. M. Webb, A. C. Dohnalkova and C. M. Hansel, Diversity of Mn oxides produced by Mn(II)-oxidizing fungi, *Geochim. Cosmochim. Acta*, 2011, **75**, 2762-2776.

22 E. C. Bonefeld-Jorgensen, M. Long, M. V. Hofmeister and A. M. Vinggaard, Endocrine-disrupting potential of bisphenol A, bisphenol A dimethacrylate, 4-*n*-nonylphenol, and 4-*n*-octylphenol in vitro: New data and a brief review, *Environ. Health Perspect.*, 2007, **115 Suppl 1**, 69-76.

23 D. Lu, C. Feng, D. Wang, Y. Lin, H. S. Ip, J. She, Q. Xu, C. Wu, G. Wang and Z. Zhou, Analysis of twenty phenolic compounds in human urine: Hydrochloric acid hydrolysis, solid-phase extraction based on K_2CO_3-treated silica, and gas chromatography tandem mass spectrometry, *Anal. Bioanal. Chem.*, 2015, **407**, 4131-4141.

24 D. Montes-Grajales, M. Fennix-Agudelo and W. Miranda-Castro, Occurrence of personal care products as emerging chemicals of concern in water resources: A review, *Sci. Total Environ.*, 2017, **595**, 601-614.

25 T. Pollock, R. E. Weaver, R. Ghasemi and D. deCatanzaro, A mixture of five endocrine-disrupting chemicals modulates concentrations of bisphenol A and estradiol in mice, *Chemosphere*, 2018, **193**, 321-328.

26 M. L. Davi and F. Gnudi, Phenolic compounds in surface water, *Water Res.*, 1999, **33**, 3213-3219.

27 N. Shaikh, H. Zhang, K. Rasamani, K. Artyushkova, A. S. Ali and J. M. Cerrato, Reaction of bisphenol A with synthetic and commercial $MnO_{x(s)}$: Spectroscopic and kinetic study, *Environ. Sci. Process. Impacts*, 2018, **20**, 1046-1055.

28 H. Zhang, W. R. Chen and C. H. Huang, Kinetic modeling of oxidation of antibacterial agents by manganese oxide, *Environ. Sci. Technol.*, 2008, **42**, 5548-5554.

29 A. S. Pavitt, E. J. Bylaska and P. G. Tratnyek, Oxidation potentials of phenols and anilines: Correlation analysis of electrochemical and theoretical values, *Environ. Sci. Process. Impacts*, 2017, **19**, 339-349.

30 S. Canonica and P. G. Tratnyek, Quantitative structure-activity relationships for oxidation reactions of organic chemicals in water, *Environ. Toxicol. Chem.*, 2003, **22**, 1743-1754.

31 C. Costentin, M. Robert and J. M. Saveant, Concerted proton-electron transfers: Electrochemical and related approaches, *Acc. Chem. Res.*, 2010, **43**, 1019-1029.

32 K. Lin, W. Liu and J. Gant, Oxidative removal of bisphenol A by manganese dioxide: Efficacy, products, and pathways, *Environ. Sci. Technol.*, 2009, **43**, 3860-3864.

33 K. Rubert and J. A. Pedersen, Kinetics of oxytetracycline reaction with a hydrous manganese oxide, *Environ. Sci. Technol.*, 2006, **40**, 7216-7221.

34 L. Ukrainczyk and M. B. Mcbride, Oxidation and dechlorination of chlorophenols in dilute aqueous suspensions of manganese oxides - reaction products, *Environ. Toxicol. Chem.*, 1993, **12**, 2015-2022.
35 S. Balgooyen, P. J. Alaimo, C. K. Remucal and M. Ginder-Vogel, Structural transformation of MnO_2 during the oxidation of bisphenol A, *Environ. Sci. Technol.*, 2017, **51**, 6053-6062.
36 S. Balgooyen, G. Campagnola, C. K. Remucal and M. Ginder-Vogel, Impact of bisphenol A influent concentration and reaction time on MnO_2 transformation in a stirred flow reactor, *Environ. Sci. Process. Impacts*, 2019, **21**, 19-27.
37 J. Huang, S. Zhong, Y. Dai, C. C. Liu and H. Zhang, Effect of MnO_2 phase structure on the oxidative reactivity toward bisphenol A degradation, *Environ. Sci. Technol.*, 2018, **52**, 11309-11318.
38 J. Klausen, S. B. Haderlein and R. P. Schwarzenbach, Oxidation of substituted anilines by aqueous MnO_2: Effect of co-solutes on initial and quasi-steady-state kinetics, *Environ. Sci. Technol.*, 1997, **31**, 2642-2649.
39 S. Laha and R. G. Luthy, Oxidation of aniline and other primary aromatic amines by manganese dioxide, *Environ. Sci. Technol.*, 1990, **24**, 363-373.
40 J. W. Park, J. Dec, J. E. Kim and J. M. Bollag, Effect of humic constituents on the transformation of chlorinated phenols and anilines in the presence of oxidoreductive enzymes or birnessite, *Environ. Sci. Technol.*, 1999, **33**, 2028-2034.
41 A. J. Salter-Blanc, E. J. Bylaska, M. A. Lyon, S. C. Ness and P. G. Tratnyek, Structure-activity relationships for rates of aromatic amine oxidation by manganese dioxide, *Environ. Sci. Technol.*, 2016, **50**, 5094-5102.
42 N. Shaikh, S. Taujale, H. Zhang, K. Artyushkova, A. S. Ali and J. M. Cerrato, Spectroscopic investigation of interfacial interaction of manganese oxide with triclosan, aniline, and phenol, *Environ. Sci. Technol.*, 2016, **50**, 10978-10987.
43 H. Zhang and C. H. Huang, Oxidative transformation of triclosan and chlorophene by manganese oxides, *Environ. Sci. Technol.*, 2003, **37**, 2421-2430.
44 M. D. R. Pizzigallo, P. Ruggiero, C. Crecchio and R. Mininni, Manganese and iron-oxides as reactants for oxidation of chlorophenols, *Soil Sci. Soc. Am. J.*, 1995, **59**, 444-452.
45 P. G. Tratnyek, E. J. Bylaska and E. J. Weber, In silico environmental chemical science: Properties and processes from statistical and computational modelling, *Environ. Sci. Process. Impacts*, 2017, **19**, 188-202.
46 A. Cherkasov, E. N. Muratov, D. Fourches, A. Varnek, Baskin, II, M. Cronin, J. Dearden, P. Gramatica, Y. C. Martin, R. Todeschini, V. Consonni, V. E. Kuz'min, R. Cramer, R. Benigni, C. Yang, J. Rathman, L. Terfloth, J. Gasteiger, A. Richard and A. Tropsha, QSAR modeling: Where have you been? Where are you going to?, *J. Med. Chem.*, 2014, **57**, 4977-5010.
47 Y. Lee and U. von Gunten, Quantitative structure-activity relationships (QSARs) for the transformation of organic micropollutants during oxidative water treatment, *Water Res.*, 2012, **46**, 6177-6195.
48 W. A. Arnold, Y. Oueis, M. O'Connor, J. E. Rinaman, M. G. Taggart, R. E. McCarthy, K. A. Foster and D. E. Latch, QSARs for phenols and phenolates: Oxidation potential as a predictor of reaction rate constants with photochemically produced oxidants, *Environ. Sci. Process. Impacts*, 2017, **19**, 324-338.
49 J. W. Murray, The surface chemistry of hydrous manganese dioxide, *J. Colloid Interf. Sci.*, 1974, **46**, 357-371.

50 A. Manceau, M. A. Marcus and S. Grangeon, Determination of mn valence states in mixed-valent manganates by XANES spectroscopy, *Am. Mineral.*, 2012, **97**, 816-827.
51 M. Kosmulski, Isoelectric points and points of zero charge of metal (hydr)oxides: 50 years after Parks' review, *Adv. Colloid Interface Sci.*, 2016, **238**, 1-61.
52 T. Mahmood, M. T. Saddique, A. Naeem, P. Westerhoff, S. Mustafa and A. Alum, Comparison of different methods for the point of zero charge determination of NiO, *Ind. Eng. Chem. Res.*, 2011, **50**, 10017-10023.
53 *CRC handbook of chemistry and physics*, CRC Press LLC, Boca Raton, FL 95th edn., 2014-2015.
54 S. C. Ying, B. D. Kocar, S. D. Griffis and S. Fendorf, Competitive microbially and Mn oxide mediated redox processes controlling arsenic speciation and partitioning, *Environ. Sci. Technol.*, 2011, **45**, 5572-5579.
55 W. S. Yao and F. J. Millero, Adsorption of phosphate on manganese dioxide in seawater, *Environ. Sci. Technol.*, 1996, **30**, 536-541.
56 C. Hansch, A. Leo and R. W. Taft, A survey of hammett substituent constants and resonance and field parameters, *Chem. Review*, 1991, **91**, 165-195.
57 R. P. Schwarzenbach, P. M. Gschwend and Imboden, in *Environmental organic chemistry*, John Wiley & Sons, Inc., Hoboken, New Jersey, 2nd edn., 2003, ch. 8, 245-274.
58 G. B. Barlin and D. D. Perrin, Prediction of the strengths of organic acids, *Q. Rev. Chem. Soc.*, 1966, 75-101.
59 J. Clark and D. D. Perrin, Prediction of the strengths of organic bases, *Q. Rev. Chem. Soc.*, 1964, 295-320.
60 P. G. Tratnyek, in *Perspectives in environmental chemistry*, ed. D. Macalady, Oxford University Press, 1998, pp. 167-194.
61 M. Swain, Chemicalize.Org, *J. Chem. Inf. Model.*, 2012, **52**, 613-615.
62 M. Valiev, E. J. Bylaska, N. Govind, K. Kowalski, T. P. Straatsma, H. J. J. Van Dam, D. Wang, J. Nieplocha, E. Apra, T. L. Windus and W. de Jong, NWChem: A comprehensive and scalable open-source solution for large scale molecular simulations, *Comput. Phys. Commun.*, 2010, **181**, 1477-1489.
63 L. Zhao, Z. Yu, P. Peng, W. Huang and Y. Dong, Oxidative transformation of tetrachlorophenols and trichlorophenols by manganese dioxide, *Environ. Toxicol. Chem.*, 2009, **28**, 1120-1129.
64 Y. Wang, S. Benkaddour, F. F. Marafatto and J. Pena, Diffusion- and pH-dependent reactivity of layer-type MnO_2: Reactions at particle edges versus vacancy sites, *Environ. Sci. Technol.*, 2018, **52**, 3476-3485.
65 R. G. Lehmann, H. H. Cheng and J. B. Harsh, Oxidation of phenolic acids by soil iron and manganese oxides, *Soil Sci. Soc. Am. J.*, 1987, **51**, 352-356.
66 M. L. Colarieti, G. Toscano, M. R. Ardi and G. Greco, Jr., Abiotic oxidation of catechol by soil metal oxides, *J. Hazard. Mater.*, 2006, **134**, 161-168.
67 I. Forrez, M. Carballa, K. Verbeken, L. Vanhaecke, T. Ternes, N. Boon and W. Verstraete, Diclofenac oxidation by biogenic manganese oxides, *Environ. Sci. Technol.*, 2010, **44**, 3449-3454.
68 J. Dong, Z. LiJia, L. Hui, L. ChengShuai, G. YuanXue and S. LiNa, The oxidative degradation of 2-mercaptobenzothialzole by different manganese dioxides, *Fresen. Environ. Bull.*, 2010, **19**, 1615-1622.

69 C. S. Liu, L. J. Zhang, F. B. Li, Y. Wang, Y. Gao, X. Z. Li, W. D. Cao, C. H. Feng, J. Dong and L. N. Sun, Dependence of sulfadiazine oxidative degradation on physicochemical properties of manganese dioxides, *Ind. Eng. Chem. Res.*, 2009, **48**, 10408-10413.

70 D. Colon, E. J. Weber and G. Baughman, Sediment-associated reactions of aromatic amines 2. QSAR development, *Environ. Sci. Technol.*, 2002, **36**, 2443-2450.

71 P. G. Tratnyek, E. J. Weber and R. P. Schwarzenbach, Quantitative structure-activity relationships for chemical reductions of organic contaminants, *Environ. Toxicol. Chem.*, 2003, **22**, 1733-1742.

72 J. L. Devore, *Probability & statistics for engineering and the sciences*, Brooks/Cole, Boston, MA, 8 edn., 2012.

73 N. Frimayanti, M. L. Yam, H. B. Lee, R. Othman, S. M. Zain and N. A. Rahman, Validation of quantitative structure-activity relationship (QSAR) model for photosensitizer activity prediction, *Int. J. Mol. Sci.*, 2011, **12**, 8626-8644.

74 P. Gramatica, On the development and validation of QSAR models, *Methods Mol. Biol.*, 2013, **930**, 499-526.

75 R. Veerasamy, H. Rajak, A. Jain, S. Sivadasan, C. P. Varghese and R. K. Agrawal, Validation of QSAR models - strategies and importance, *Int. J. Drug Design Discov.*, 2011, **2**, 511-519.

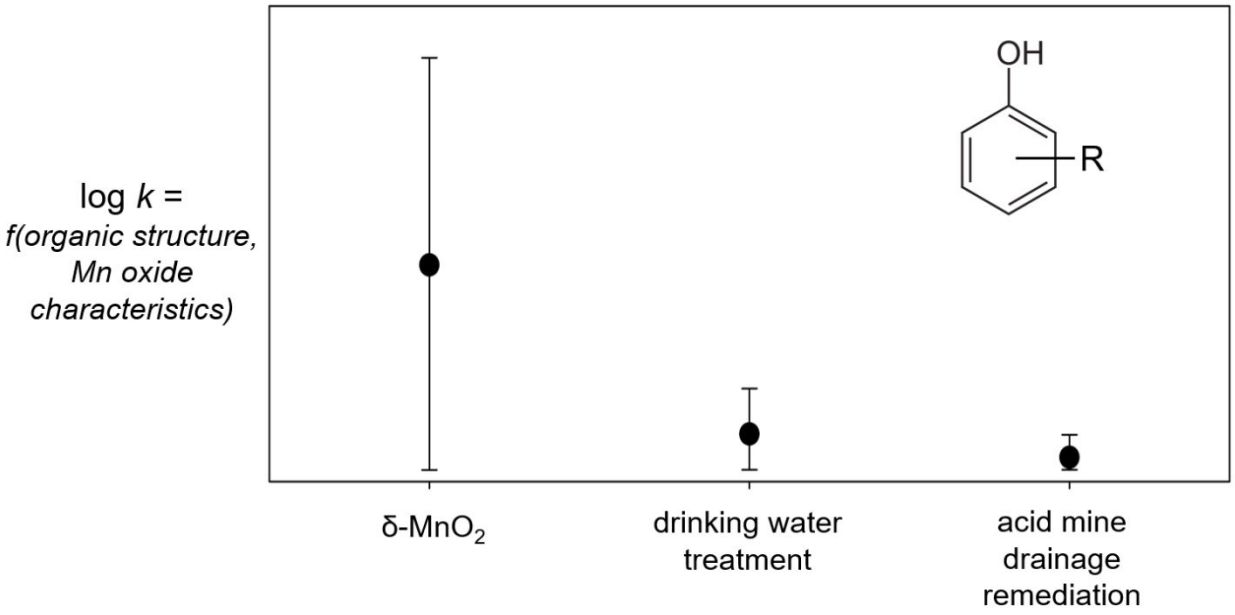

Phenolic substituents and manganese oxide characteristics influence oxidation kinetics and mechanism, as well as the utility of QSARs.